PiscoMed Publishing

doi: 10.18282/iac.v6i1.569

Original Research Article

Speed control of PMBLDC motor drive powered by solar PV array using P, PI, and PID controllers: A comparison study

Satish Kumar Doniparthi[1], S. B. Ron Carter[2], Amit Vilas Sant[3], Ali Moghassemi[4,*]

[1] *New Horizon College of Engineering/E.E.E Department, Bangalore 560078, India*

[2] *Rajalakshmi Engineering College/E.E.E Department, Chennai 600001, India*

[3] *Pandit Deendayal Energy University, Gujarat 382425, India*

[4] *Holcombe Department of Electrical and Computer Engineering, Clemson University, Clemson 29634, USA*

*** Corresponding author:** Ali Moghassemi, amoghas@clemson.edu

Abstract: Because of their high efficiency, better starting torque, and minimal electrical noise, permanent magnet brushless DC (PMBLDC) motors are frequently used in a variety of industrial applications. The speed of PMBLDC motors is controlled by a variety of controllers. In this study, P, PI, and PID controllers are used to compare the speed control of a permanent magnet brushless DC motor drive powered by solar PV arrays. The Perturb & Observe (P&O) technique is used to find the MPPT. The drive system's simulation results for various operation modes, such as constant and variable load circumstances, are examined and evaluated. When using a PID controller instead of a P or PI controller, the drive performs better at controlling speed. The MATLAB/Simulink software was used to model, control, and simulate the permanent magnet brushless DC motor drive. The whole drive system is put into operation with the help of the dSPACE MicroLab Box 1202.

Keywords: MPPT; PMBLDC motor; PID controller; solar PV array; speed control; dSPACE

Received: 10 March 2023; **Accepted:** 4 May 2023; **Available online:** 21 July 2023

1. Introduction

Renewable energy sources are becoming increasingly popular due to their low environmental impact and sustainable nature. Solar photovoltaic (PV) arrays are one such source of renewable energy that has gained significant attention in recent years. However, due to the intermittent nature of solar energy, efficient utilization of this energy source requires the use of a suitable energy storage system and an efficient control strategy. Furthermore, renewable energy sources offer a viable alternative for reducing global warming by reducing carbon emissions. Increased usage of renewable energy sources would help the globe achieve long-term sustainability. One of the most accessible forms of energy to use among several RE sources is solar energy[1]. To get the most power out of a solar PV array, Maximum Power Point Tracking (MPPT) is required. The most fundamental MPPT approaches are fractional open-circuit voltage and fractional short-circuit current[2]. They do, however, have a decreased tracking efficiency. The Perturb and observe (P&O) approach is a popular MPPT methodology with outstanding tracking efficiency. It is used in this research because of its tracking fidelity even when the sun irradiation changes abruptly[3].

A permanent magnet brushless DC (PMBLDC) motor is a permanent magnet synchronous motor. **Figure 1** shows the block diagram of the solar PV array-powered permanent magnet brushless DC motor drive[4].

PMBLDC motors are widely used in various applications due to their high efficiency, low maintenance, and reliable operation. PMBLDC motors are often used in Solar PV-powered applications, such as water pumps, air compressors, and fans. However, controlling the speed of a PMBLDC motor drive powered by a solar PV array is a challenging task due to the fluctuating nature of solar energy. PMBLDC motors are known for their superior speed-to-torque relationships, high power density, extended operational life, quiet operation, and control qualities. Because of their many advantages, these motors are widely utilized in industry, and several control methods for controlling the speed of these motors have been proposed[5].

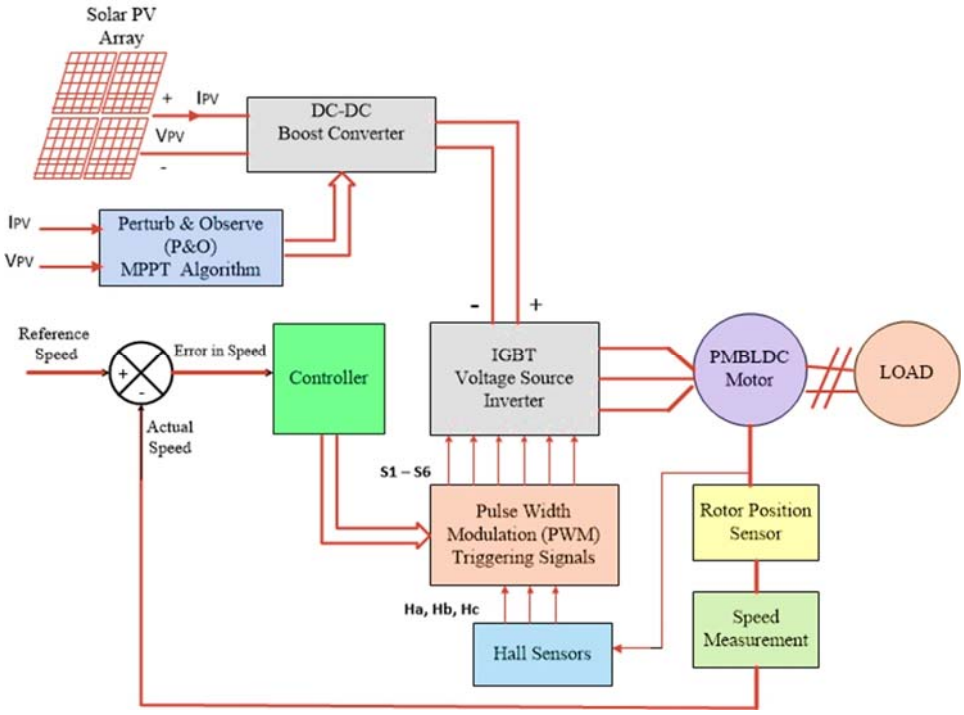

Figure 1. Block diagram of solar PV array powered permanent magnet brushless DC (PMBLDC) motor-drive.

To improve the performance of PMBLDC motors, intelligent algorithms such as particle swarm, fuzzy logic control, differential evolution, neural network, neuro-fuzzy, and sliding mode control can use to alter the gains of the P, PI, and PID controllers[6,7]. In this study, under constant and variable load conditions, a comparison of Speed control of solar PV array with MPPT P&O algorithm powered permanent magnet brushless DC motor drive utilizing Proportional (P), Proportional-Integral (PI), and Proportional-Integral-Derivative (PID) controllers are observed in MATLAB/SIMULINK software, and the results are analyzed and compared for each controller type. The permanent magnet brushless DC motor drive with mechanical load is developed on MATLAB/SIMULINK platform and then implemented on the dSPACE MicroLab Box 1202 platform with a sampling frequency of 10 kHz.

The paper is organized as follows: Section 2 presents the modelling of the solar PV array; Section 3 presents the boost DC-DC converter; Section 4 presents the modelling of the PMBLDC motor; Section 5 discusses the different controller techniques (P, PI, and PID); Section 6 shows the simulation results for solar PV array powered speed control of PMBLDC motor drive with P, PI, and PID controller under constant and variable load conditions; Section 7 presents the hardware results and then Section 8 presents the conclusion of the paper.

2. Modeling of solar PV array

Using light energy, a solar photovoltaic system generates electricity. Arrays of solar cells are commonly used in solar PV systems[8]. PV array output voltage, current, and power are all affected by an amount of solar irradiation in the area where they are installed. A solar PV cell is a voltage-controlled current source that is interconnected in parallel with a diode[9].

As shown in **Figure 2**, the equivalent circuit of a PV cell contains the following components: V_{PV} and I_{PV} represent the PV cell current and voltage, respectively, I_{ph} represents the PV cell photocurrent, V_d represents the voltage across the diode, R_s and R_{sh} represent the series and shunt resistances of the cell, and I_{sh} represents the current flowing through the shunt resistance R_{sh}, which is extremely large.

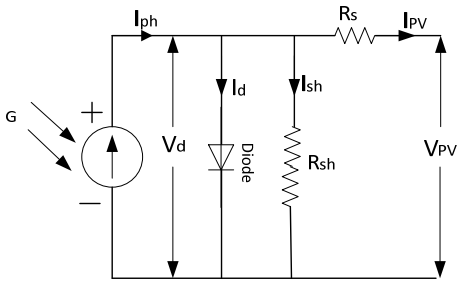

Figure 2. Equivalent circuit of solar PV cell.

By using Kirchhoff's current law (KCL), PV module current can be written as:

$$I_{PV} = I_{ph} - I_d - I_{sh} \tag{1}$$

$$I_{PV} = \left(I_{sc}\frac{G}{G^*}\right) - \left\{I_o\left(e^{\frac{v_d}{v_t}} - 1\right)\right\} - \frac{v_d}{R_{sh}} \tag{2}$$

$$V_d = V_{PV} + I_{PV}R_s \tag{3}$$

$$V_t = \frac{(N_s kT)}{q} \tag{4}$$

where, G is solar irradiance (W/m^2), G^* is nominal irradiance, I_{sc} denotes the short circuit current of the module, I_d denotes a current flowing through the diode, T denotes the temperature of the p-n junction in Kelvin, I_o denotes diode saturation current, V_t denotes thermal voltage, N_s denotes the total number of cells connected in a series, k is Boltzmann constant (1.38×10^{-23} J/K), and q is the charge of an electron (1.6×10^{-19} C).

Table 1. Solar PV array parameters.

Parameter	Value
Strings that are parallel	66
Modules connected in a series per string	5
Open circuit voltage (V_{oc})	64.2 V
Maximum power point voltage (V_{mp})	54.7 V
Maximum power	305.226 W
Maximum power point current (I_{mp})	5.58 A
Short-circuit current (I_{sc})	5.96 A

Current vs. Voltage (I-V) and Power vs. Voltage (P-V) curves of solar PV array as shown in **Figure 3**. When it comes to solar panels, there is only one operational point. These maximum power points (VPVs) can only be achieved if the operating point of the PV generator is adjusted at the inflection point of the IPV curve[10].

Maximum power point (MPP) is a term used to describe a PV array's optimal operating condition, and the process of running a module at this point is called maximum power point tracking (MPPT).

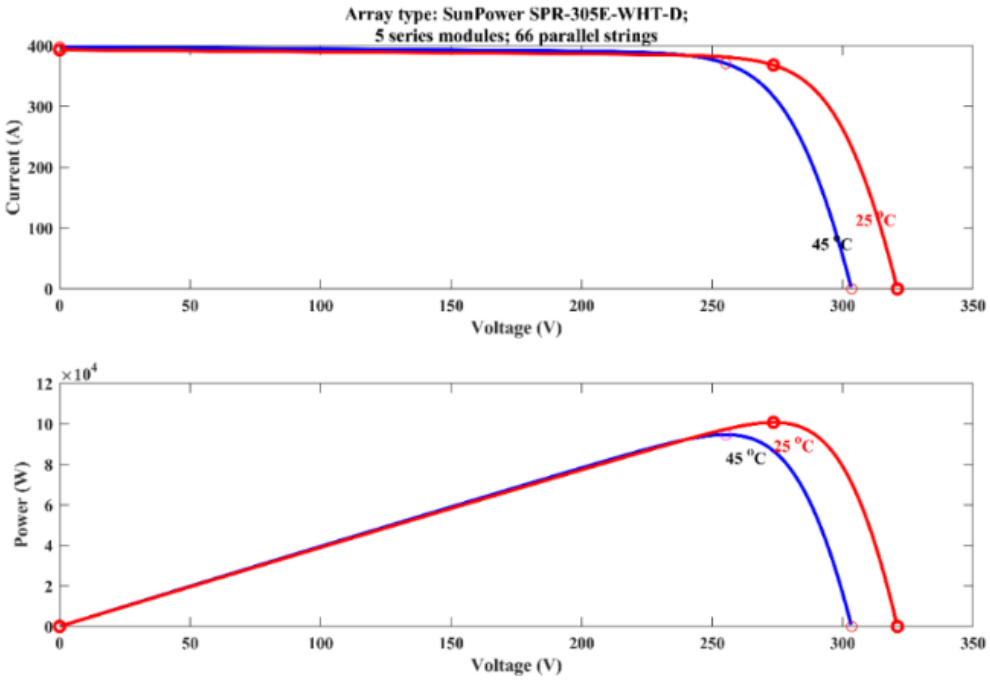

Figure 3. I-V and P-V curves of solar PV array.

The Perturb and observe (P&O) method is employed in this paper for detecting MPPT[11,12]. **Figure 4** shows the flowchart for the P&O algorithm. This approach uses the PV output terminal voltage to increase or decrease periodically, and the current cycle's output power is to be compared to the previous cycle's output. Once the direction of current change is understood, the current is modulated at a steady rate. Faster response times can be achieved with less volatility in the steady-state by adjusting this rate. As a result, it oscillates about the maximum power point due to the perturbing process of finding the maximum power point.

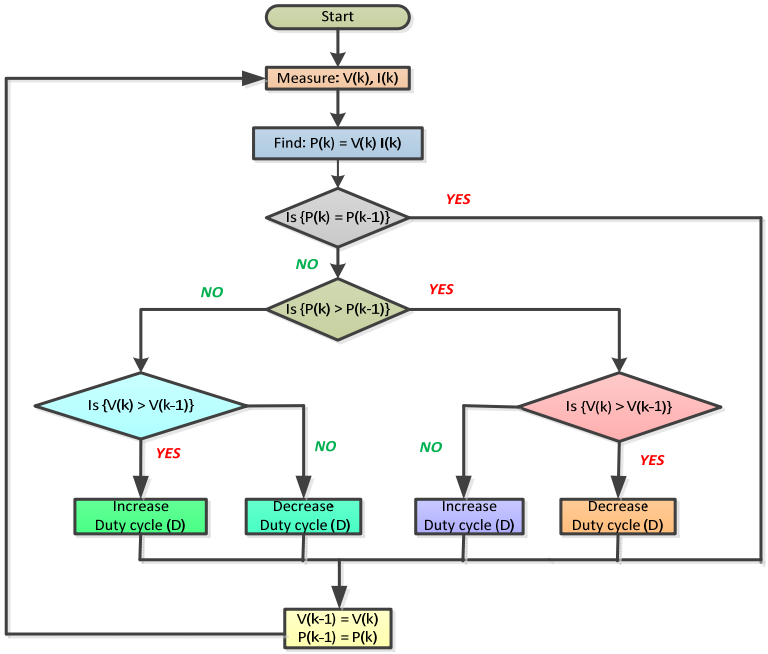

Figure 4. Perturb and observe (P&O) algorithm.

3. Boost DC-DC converter

Boosting inductor (L), controlled switch (IGBT), diode, and capacitor (C) are all components of a DC-DC boost converter as shown in **Figure 5**. The following equations are used to design the inductor and capacitor of the boost converter[13].

$$\Delta I_L = \frac{(V_i)min.D}{f_s.L} \tag{5}$$

$$L = \frac{V_i(V_o - V_i)}{\Delta I_L.f_s.V_o} \tag{6}$$

$$C = \frac{I_o.D}{\Delta v_o.f_s} \tag{7}$$

where, f_s denotes switching frequency, D denotes duty cycle, $(V_i)_{min}$ denotes minimum input voltage, V_i denotes input voltage, V_o denotes output voltage, Δv_o denotes the estimated output ripple voltage, ΔI_L denotes the estimated inductor ripple current, C denotes capacitor, I_o denotes the output current and L denotes inductor.

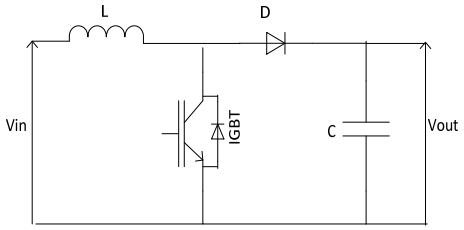

Figure 5. Boost DC-DC converter.

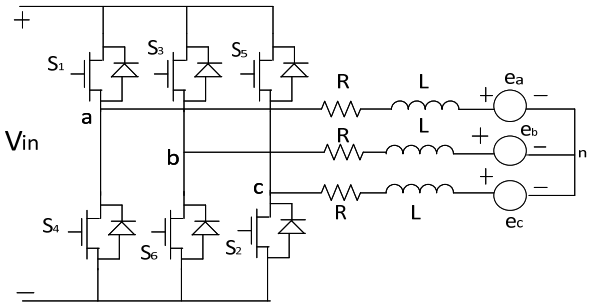

Figure 6. Equivalent circuit of PMBLDC motor.

Table 2. Boost DC-DC converter parameters.

Parameters	Value
Inductance (L)	5 mH
Input capacitance (C_{in})	100 µF
Output capacitance (C_{out})	12,000 µF
Switching frequency (f_{sw})	5 kHz
Output voltage	320 V
Output current	25

4. Modeling of PMBLDC motor

In recent years, permanent magnet brushless DC (PMBLDC) motors have become increasingly popular in a wide range of industrial and domestic applications. This type of permanent magnet synchronous motor has a rotor with permanent magnets and a trapezoidal back-EMF. Stator phase windings are fed from a DC

power supply via S1–S6 switching devices, and their sequence is determined by the rotor's position[14]. The equivalent circuit of the PMBLDC motor is depicted in **Figure 6**.

When using an Insulated-Gate Bipolar Transistor (IGBT) three-phase Voltage Source Inverter (VSI) to control a PMBLDC motor, the inverter needs to know where the rotor is at all times to provide the correct commutation sequence. It is possible to use Hall effect sensors for this purpose. PMBLDC motor is powered by an IGBT three-phase VSI with a "six-step commutation or Trapezoidal control" function. Each phase has a 120-degree electrical conductivity gap between it and the next. Conducting stages S5–S6 are followed by S1–S6, S1–S2, and so on, with each conducting stage being referred to as one step in the commutation phase conductivity sequence[15]. As a result, the third phase is left inactivated in each step. Each cycle of commutation ensures that the inverter is in phase with the back-EMF, resulting in maximum torque.

Table 3. PMBLDC motor parameters.

Parameter	Value
Resistance of stator phase (R_s)	10.91 Ω
The inductance of stator phase (L_s)	30.01 e–3 H
Number of phases	3
Moment of inertia (J)	2 e–4 Kg.m^2
Viscous damping (F)	1 e–3 N.m.s
Pole pairs	4
Rated voltage	300 V
Rated current	20 A
Rated speed	3000 R.P.M
Voltage constant	137
Torque constant	1.3

The stator phase resistance and stator phase self-inductance are identical because the structure of the three stator windings is symmetrical, i.e.,

$$R_a = R_b = R_c = R \tag{8}$$

$$L_{aa} = L_{bb} = L_{cc} = L \tag{9}$$

and the mutual inductance between three-phase stator windings is the same i.e., M. The following equations can be used to evaluate a PMBLDC motor:

$$v_a = Ri_a + (L - M)\frac{di_a}{dt} + e_a \tag{10}$$

$$v_b = Ri_b + (L - M)\frac{di_b}{dt} + e_b \tag{11}$$

$$v_c = Ri_c + (L - M)\frac{di_c}{dt} + e_c \tag{12}$$

where, v_a, v_b, and v_c denote phase voltages; i_a, i_b, and i_c denote phase currents; e_a, e_b, and e_c denote phase back-EMF waveforms, R denotes phase resistance, L denotes phase self-inductance, and M denotes mutual inductance between any two phases[16]. The following equations are for the back EMF:

$$e_a = k_e\theta_e\omega_r \tag{13}$$

$$e_b = k_e(\theta_e - \frac{2\Pi}{3})\omega_r \tag{14}$$

$$e_c = k_e(\theta_e + \frac{2\Pi}{3})\omega_r \tag{15}$$

The electromagnetic torque can be calculated using the following equation:

$$T_e = \frac{(e_a i_a + e_b i_b + e_c i_c)}{\omega_r} \tag{16}$$

The equation of motion in a dynamical system is:

$$\frac{d}{dt}\omega_r = \frac{(T_e - T_L - B\omega_r)}{J} \tag{17}$$

$$\Theta_e = \left(\frac{P}{2}\right)\Theta_m \tag{18}$$

where, ω_r denotes the mechanical speed of the rotor in (rad/sec), k_e denotes back EMF constant, Θ_e denotes the rotor angle in electrical degree, Θ_m denotes the rotor angle in mechanical, B denotes damping constant, J denotes a moment of inertia for the drive, and T_L is the load torque.

5. Controllers

5.1. Proportional controller

The basic principle of a proportional controller is to apply a correction signal that is proportional to the deviation of the measured process variable from the set point. This correction signal is added to the control signal, which is the output of the controller, to adjust the process variable and bring it closer to the set point. The output of the controller in a proportional control system is proportional to the error signal.

$$k_p = 0.1$$

The transfer function of the proportional controller is:

$$G(s) = k_p \tag{19}$$

5.2. Proportional-integral (PI) controller

The system will become unstable if the proportional factor is too high. If it's too low, the system won't be able to reach the designated point in the time allotted. As a result, the proportional factor or gain of the PI controller is fine-tuned to keep the speed constant.

In a Proportional-Integral (PI) speed controller, the BLDC motor speed is compared to its reference value, and the speed error is handled[17].

$$k_p = 0.0014;\ k_i = 0.228805434597596$$

The transfer function of the PI controller is:

$$G(s) = k_p + \frac{k_i}{s} \tag{20}$$

5.3. Proportional-integral-derivative (PID) controller

The PID controller is made up of three circuit blocks: proportional, integral, and derivative. It is a common feedback control loop that corrects the difference between the measured process variable and the desired value. Small rise time, settling time, peak time, maximum overshoot percentage, and steady-state error are essential requirements for the optimal control system. The peak overshoot is decreased by utilizing a PID controller, which improves system stability[18–20]. Ziegler–Nichols's procedures are used to tune the PID values. The tuned PID values are:

$$k_p = 0.0101161945046932;\ k_i = 0.0820091011124225;\ k_d = 0.000260346693934972$$

The transfer function of the PID controller is:

$$G(s) = k_p + \frac{k_i}{s} + k_d s \tag{21}$$

where, k_p is the proportional constant, k_i is the integral constant, and k_d is the derivative constant.

6. Simulation results

The PMBLDC motor model is simulated in a Simulink environment using MATLAB. To regulate the speed of a PMBLDC motor, simulations are run for the following controllers: P, PI, and PID controllers. Different load circumstances, such as constant load and changing load, are applied to PMBLDC motors. With the use of criteria like the rise time, settling time, slew rate, pre-shoot, overshoot, and undershoot, the performance of various controllers is examined. The model was run in simulation for a total of 1.5 sec.

6.1. Under constant load conditions

The performance of the controllers is also shown at the period of 1.5 sec in **Table 4**. PID Controller performs better than other controllers. The PMBLDC motor in the MATLAB Simulink environment is made to run after tuning the P, PI, and PID controllers using Ziegler–Nichols's method, here the controller will be tuned by reducing their integral (k_i) and differential (k_d) gains. Later, only the proportional gain (k_p) is increased gradually until the system becomes unstable. The delay time taken for the output to start rising will be noted for L. Once the output reaches the set speed, the corresponding time will be noted as T. From the values of L and T, the gain values are calculated as given in Equations (22) to (24).

Gain for P controller:

$$k_p = \frac{T}{L} \tag{22}$$

Gain for PI controller:

$$k_p = 0.5\frac{T}{L};\ k_i = \frac{L}{0.3} \tag{23}$$

Gain for PID controller:

$$k_p = 1.2\frac{T}{L};\ k_i = 2L;\ k_d = 0.5L \tag{24}$$

Table 4. Under constant load conditions.

Time	Controller	Rise time (ms)	Settling time (ms)	Slew rate (ms)	Pre-shoot (%)	Overshoot (%)	Undershoot (%)
1.5 s	P	7.01	4.422	174.657	16.109	9.702	1.819
	PI	7.636	90.171	161.060	128.712	269.524	0.514
	PID	36.987	4.52	33.882	25.393	16.54	1.804

6.2. Comparison of dynamic parameters in constant load

Figures 7 to **9** provide the dynamic properties of PMBLDC motors, including three-phase stator currents, rotor speed in units of rpm, and torque (nm) for constant load application. As depicted in the figure, PID controller provides superior control over PMBLDC motor output speed when compared to other controllers. In addition, the PID controller has significantly reduced output torque ripples.

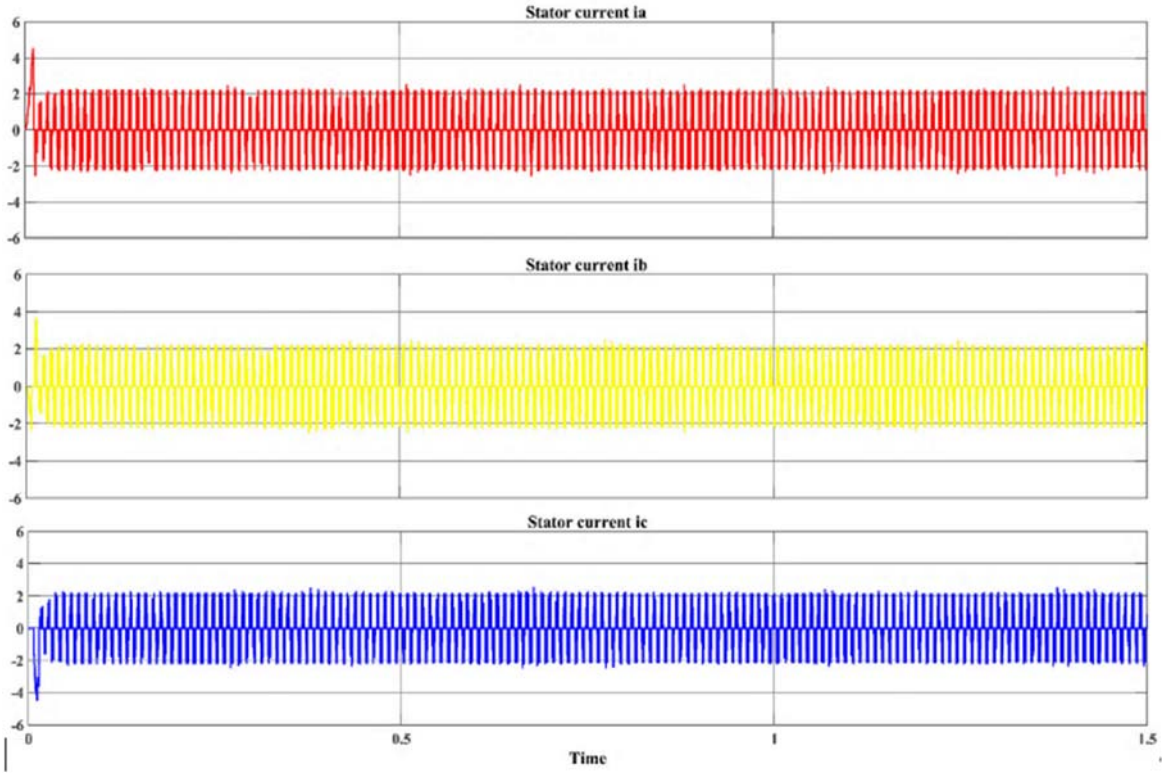

(a)

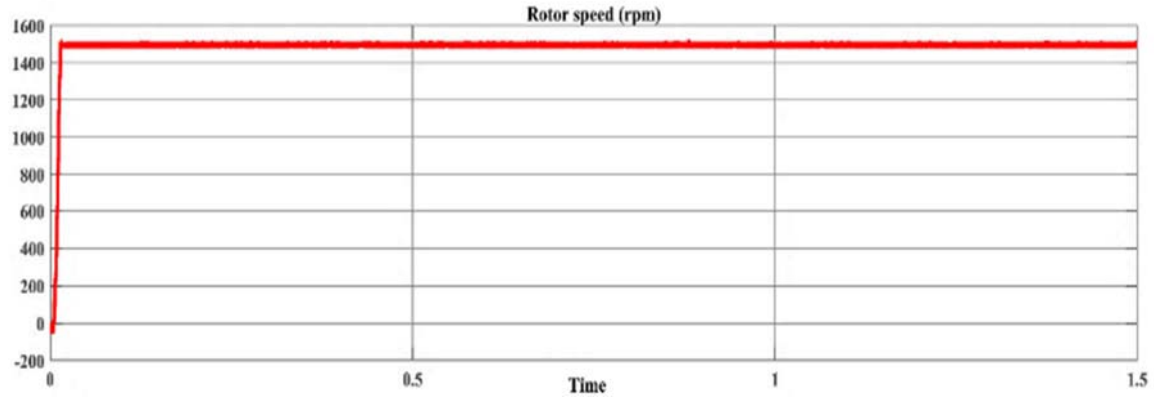

(b)

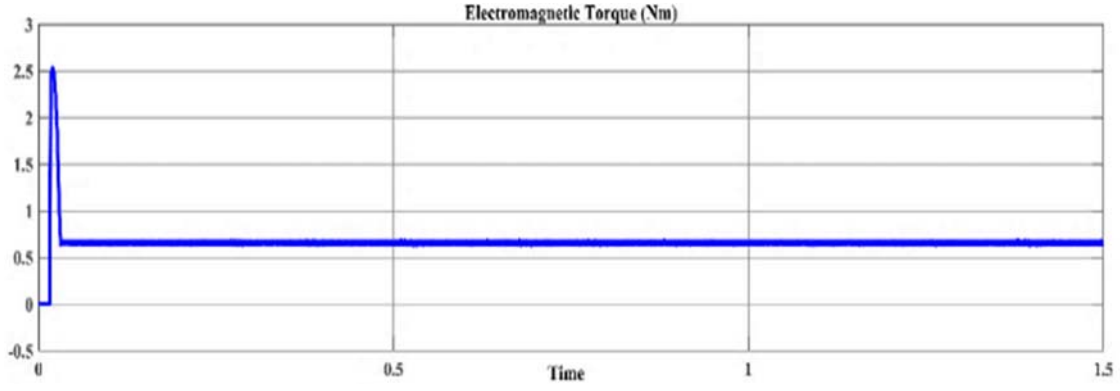

(c)

Figure 7. MATLAB simulation results for solar PV array powered speed control of PMBLDC motor drive using "P" controller under constant load conditions **(a)** stator currents, **(b)** rotor speed, and **(c)** electromagnetic torque.

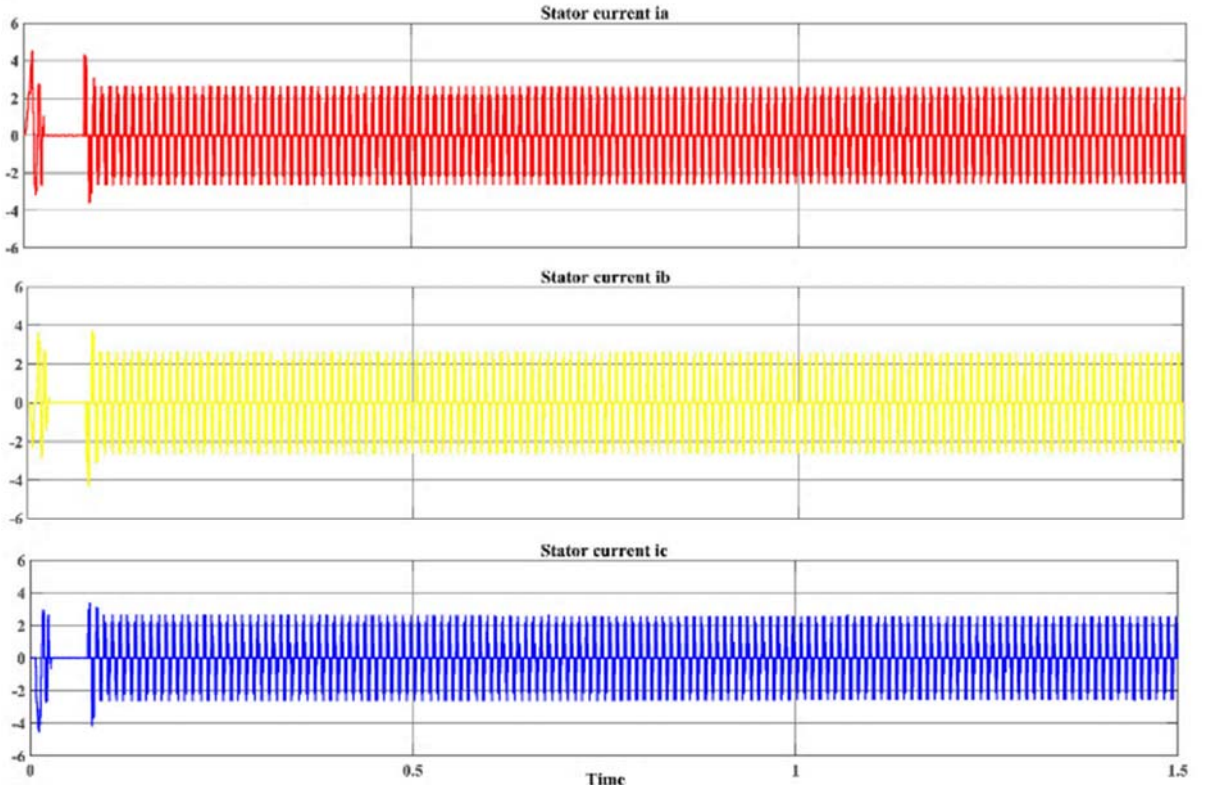

(a)

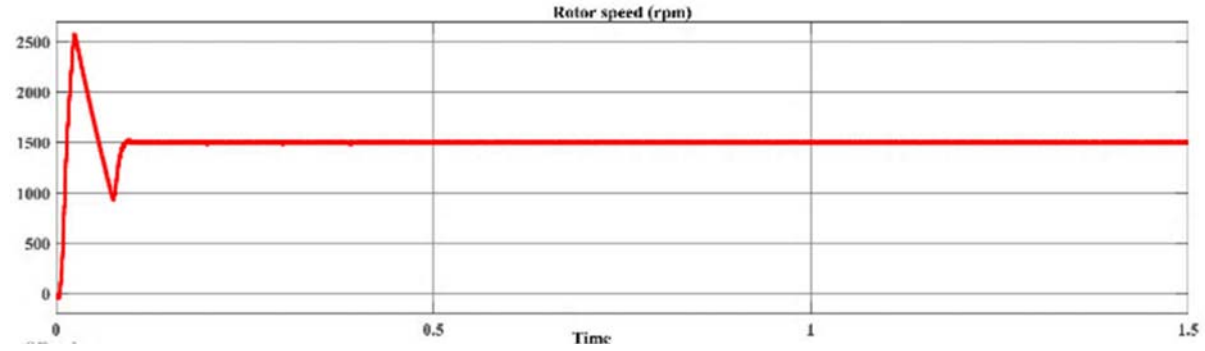

(b)

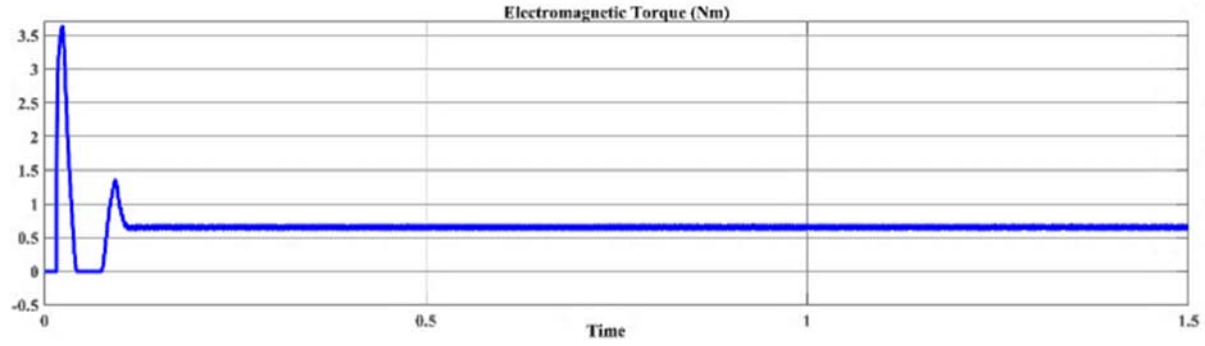

(c)

Figure 8. MATLAB simulation results for solar PV array powered speed control of PMBLDC motor drive using "PI" controller constant load conditions **(a)** stator currents, **(b)** rotor speed, and **(c)** electromagnetic torque.

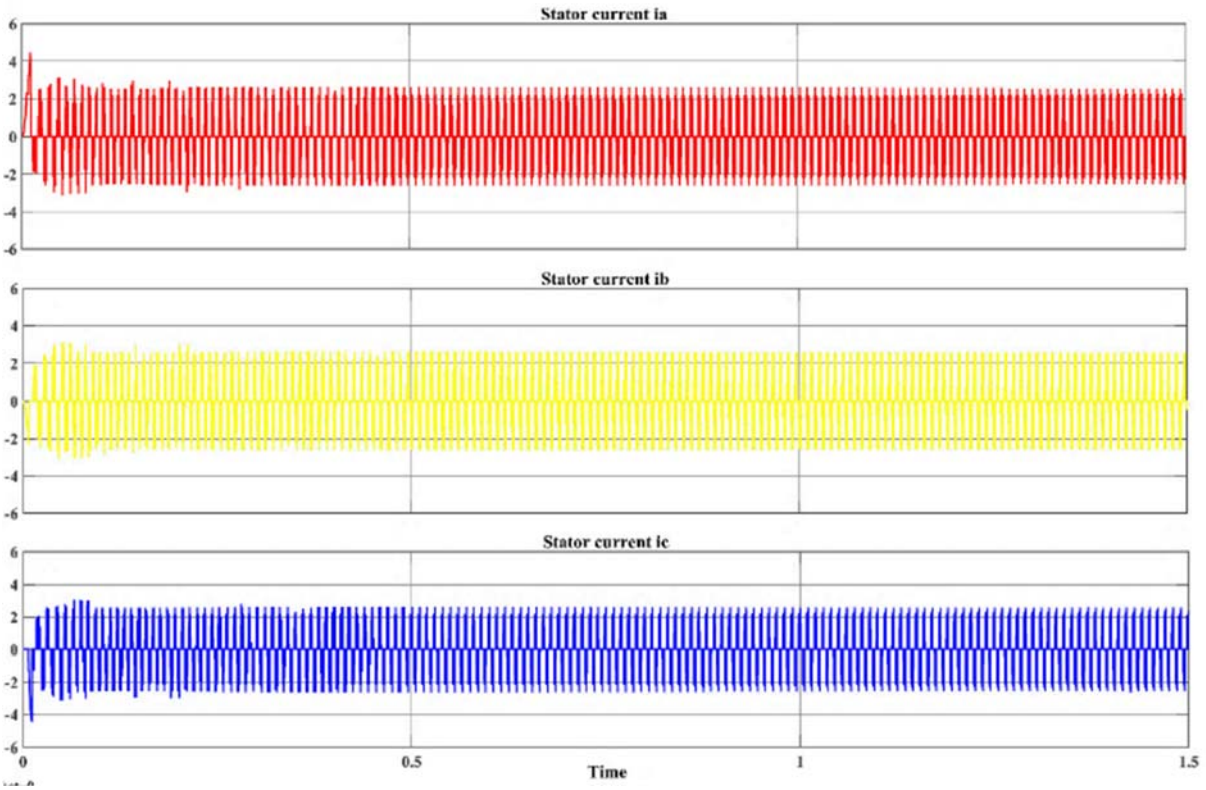

(a)

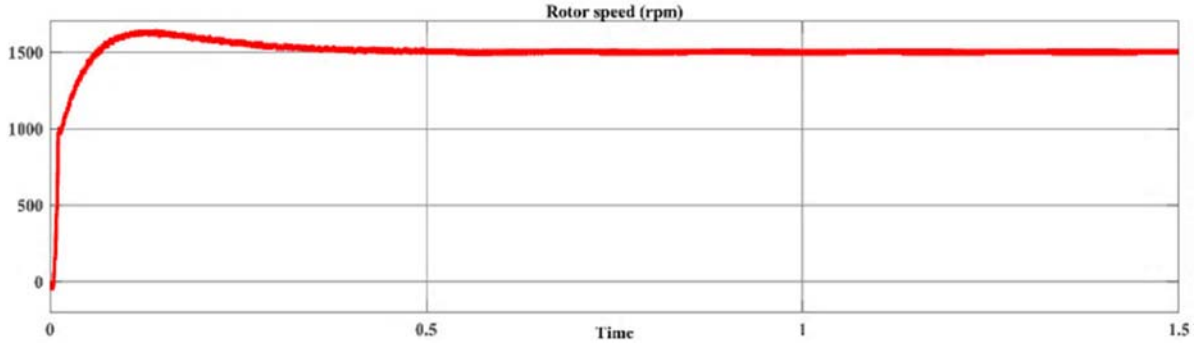

(b)

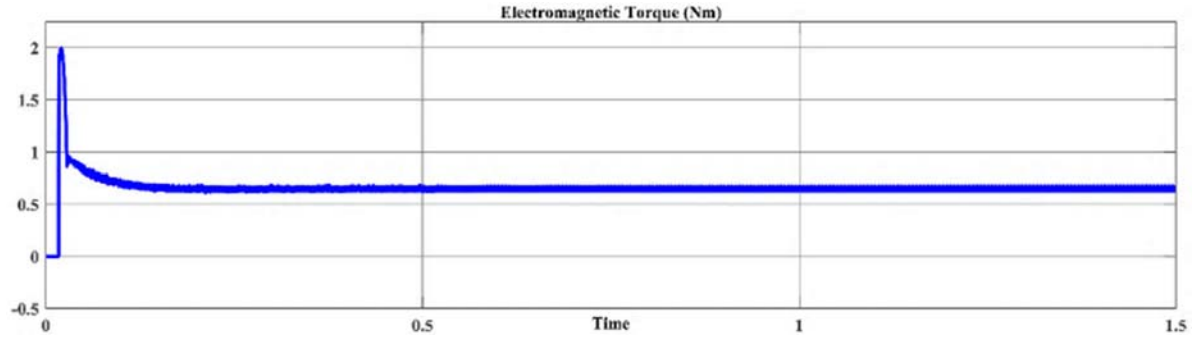

(c)

Figure 9. MATLAB simulation results for solar PV array powered speed control of PMBLDC motor drive using "PID" controller constant load conditions **(a)** stator currents, **(b)** rotor speed, and **(c)** electromagnetic torque.

6.3. Under variable load condition

The PMBLDC motor model is simulated for variable load conditions and, similarly to constant load situations and controlled by multiple controllers like P, PI, and PID. Further, rise time, settling time, slew rate, pre-shoot, overshoot, and undershoot are used to evaluate the controller's performance. **Table 5** displays the various values of the aforementioned performance criteria for various controllers under variable loading conditions.

Table 5. Under variable load conditions.

Time	Controller	Rise time (ms)	Settling time (ms)	Slew rate (ms)	Pre-shoot (%)	Overshoot (%)	Undershoot (%)
1.5 s	P	7.033	4.449	174.774	0.51	1.135	1.992
	PI	7.661	90.171	161.009	0.862	71.552	1.995
	PID	33.112	15.31	37.034	0.549	9.341	3.009

6.4. Comparison of dynamic parameters in variable load conditions

The motor's load circumstances are changing, and simulation results show the dynamic parameters, such as load currents, speed (rpm), and torque (nm). With a gradually increasing load, the corresponding current and torque increase. This results in the formation of torque ripples. Inaccurate settling speed is the result of torque ripples. According to the waveforms, the PMBLDC motor model with a PID controller outperforms the other controllers.

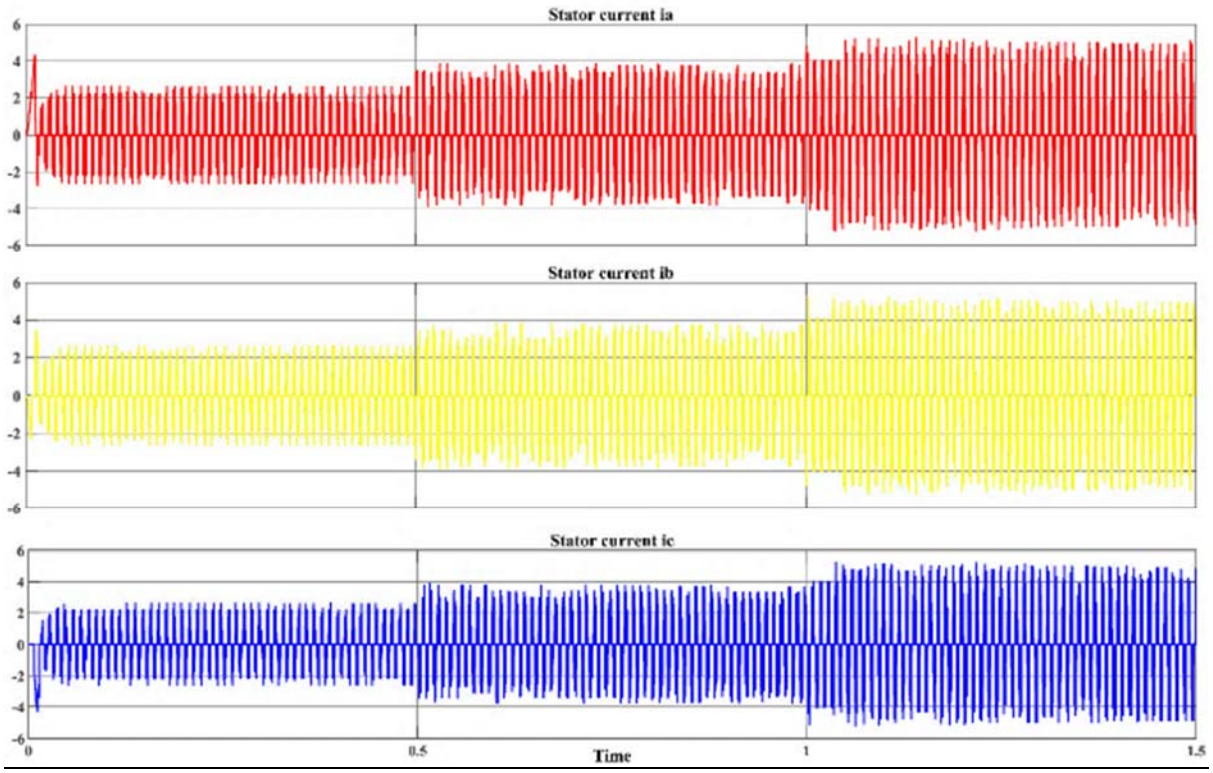

(a)

Figure 10. (*Continued*).

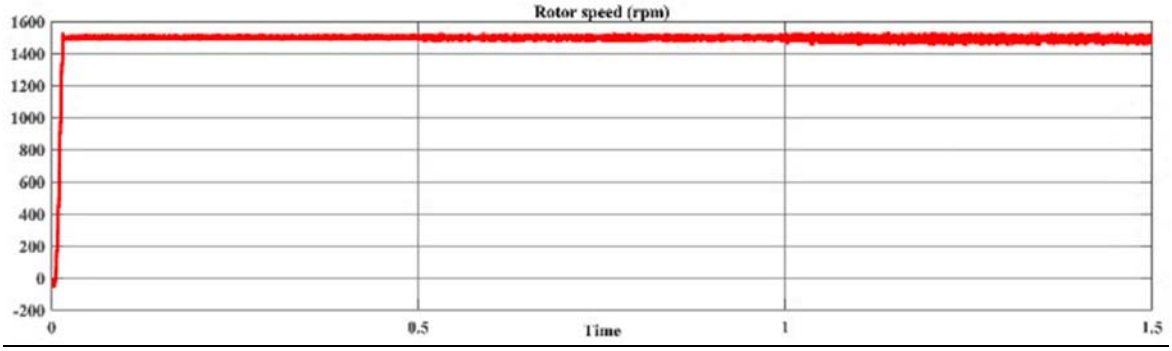

(b)

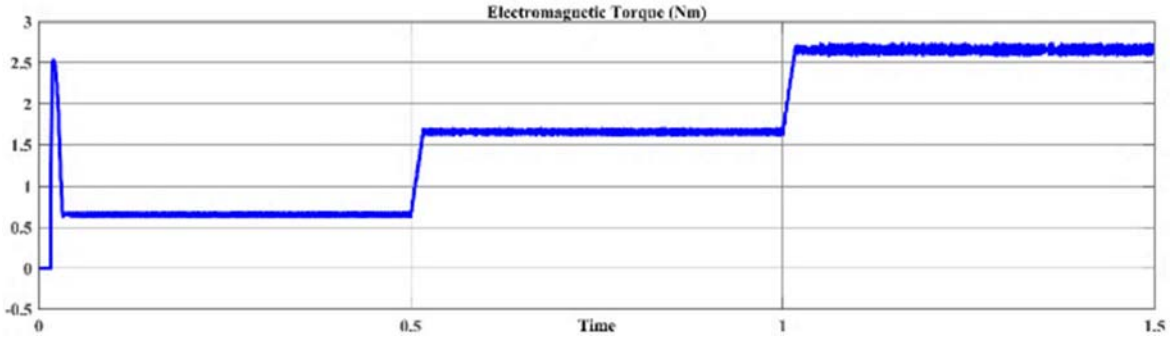

(c)

Figure 10. MATLAB simulation results for solar PV array powered speed control of PMBLDC motor drive using "P" controller under variable load conditions **(a)** stator currents, **(b)** rotor speed, and **(c)** electromagnetic torque.

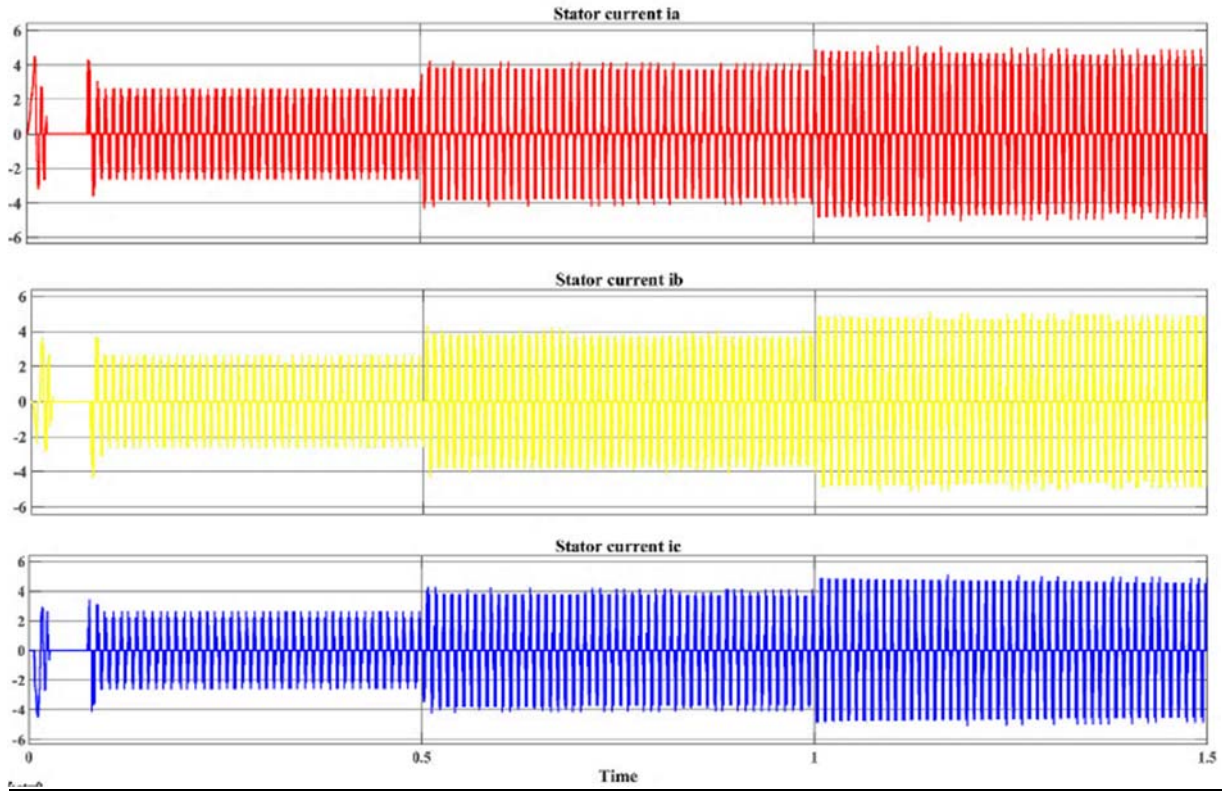

(a)

Figure 11. (*Continued*).

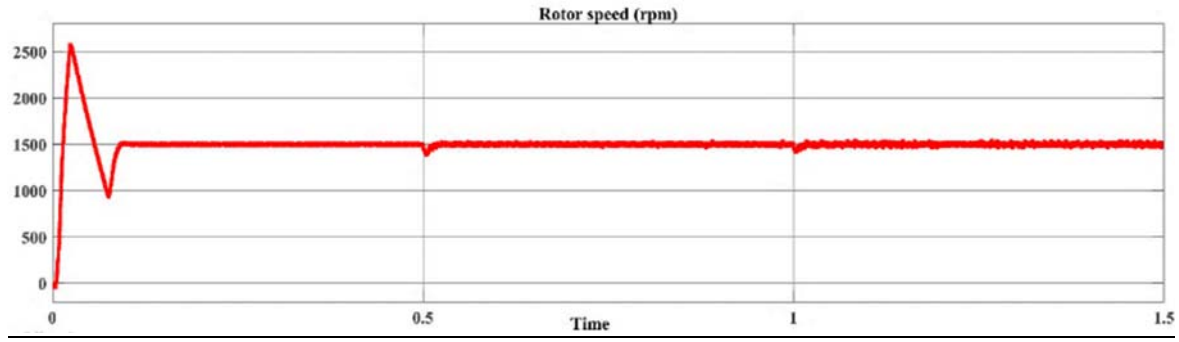

(b)

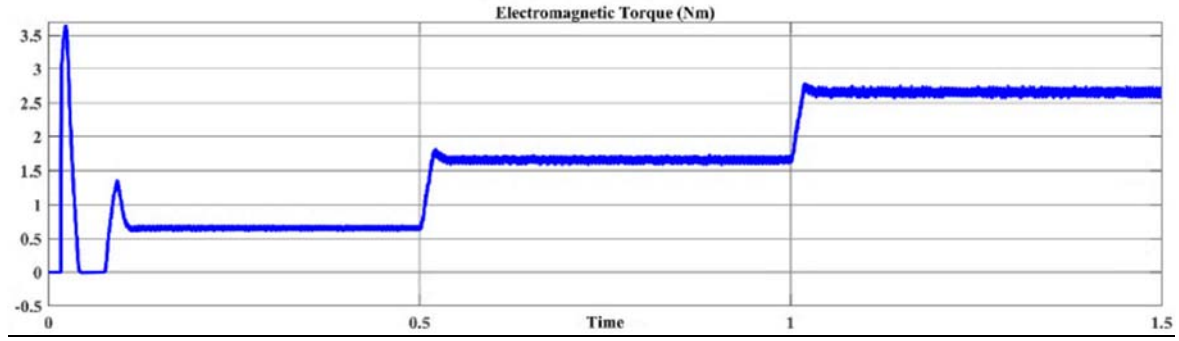

(c)

Figure 11. MATLAB simulation results for solar PV array powered speed control of PMBLDC motor drive using 'PI' controller under variable load conditions **(a)** stator currents, **(b)** rotor speed, and **(c)** electromagnetic torque.

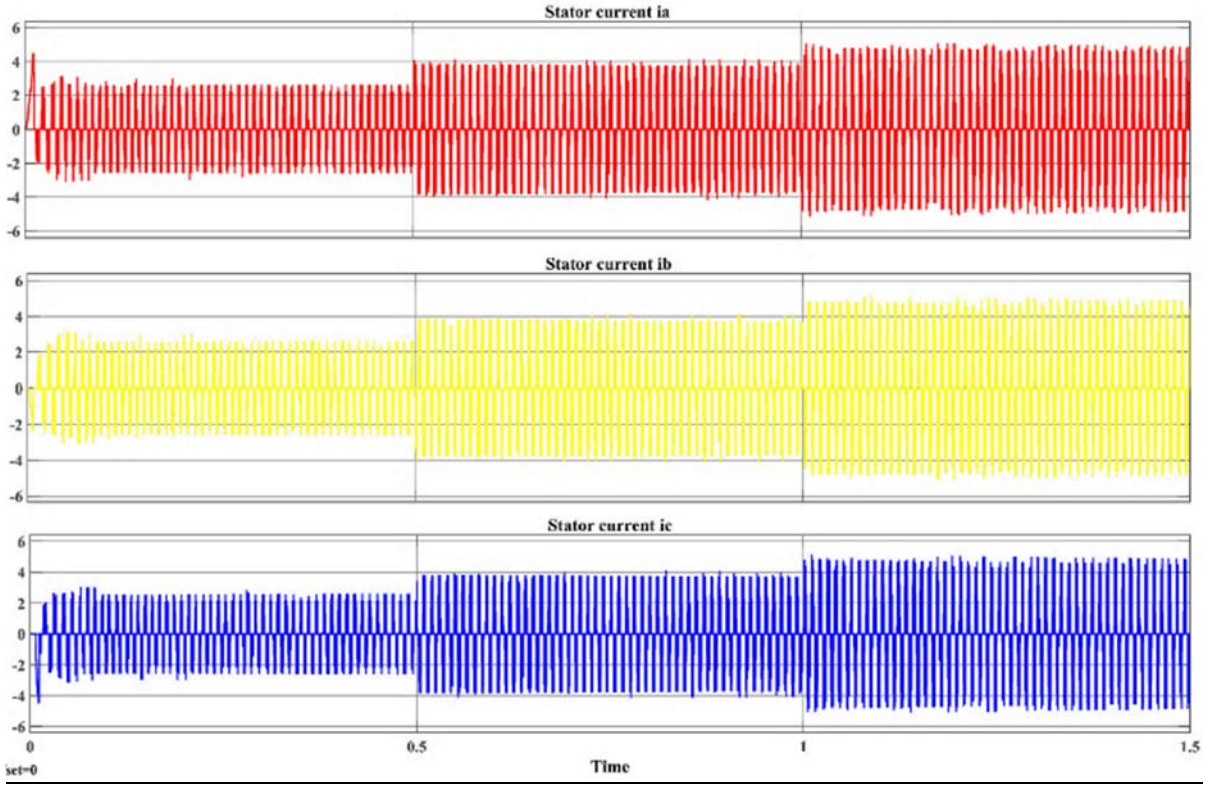

(a)

Figure 12. (*Continued*).

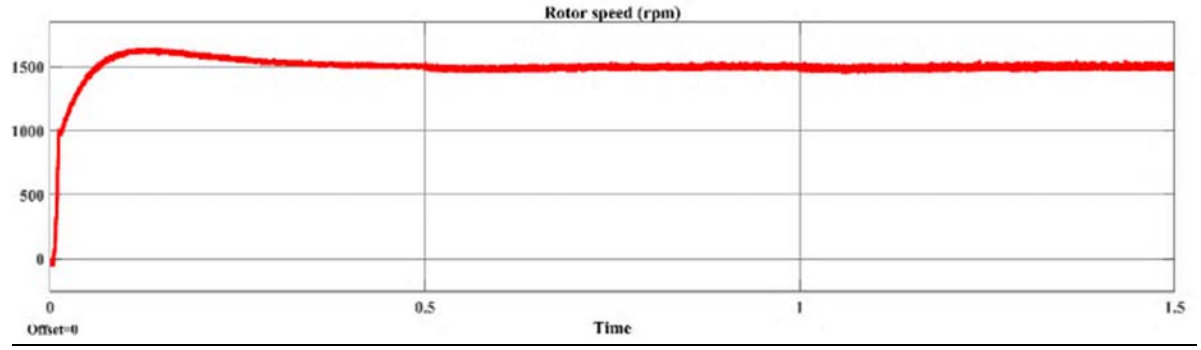

(b)

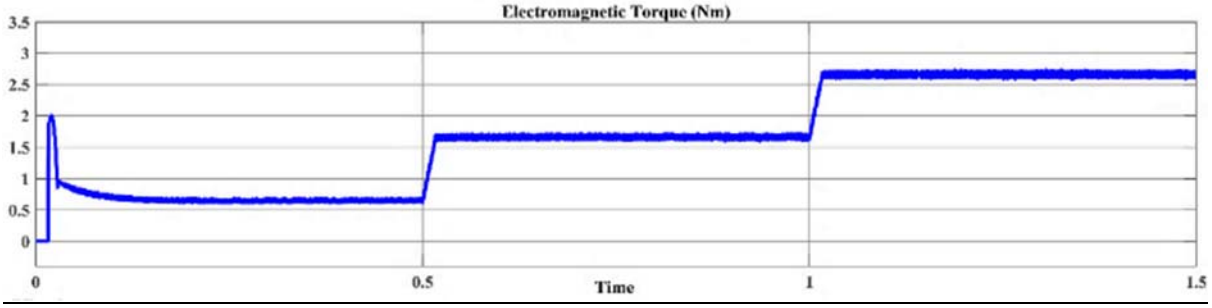

(c)

Figure 12. MATLAB simulation results for solar PV array powered speed control of PMBLDC motor drive using 'PID' controller under variable load conditions **(a)** stator currents, **(b)** rotor speed, and **(c)** electromagnetic torque.

7. Hardware results

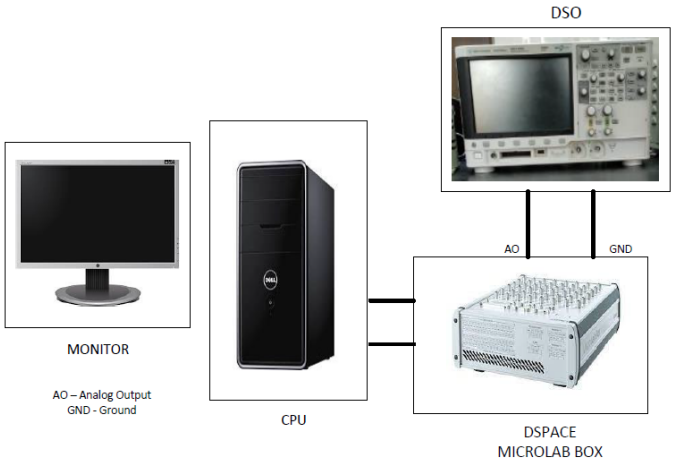

(a)

(b)

Figure 13. (a) Block diagram representation of real-time test set-up. **(b)** Experimental real-time test setup.

On the dSPACE MicroLab Box 1202 platform, the PMBLDC motor drive is put into practice for the intended application. With the appropriate adjustments made to meet the dSPACE platform, the drive system is modeled in the MATLAB/SIMULINK environment. The PMBLDC drive's performance under various circumstances is examined, and the relevant data is captured on a digital storage oscilloscope. The drive's outer speed and inner current loops, as well as the logic for PWM generation and decoding, make up the control system. **Figure 13** shows the block diagram representation of real-time test set-up.

Figure 14(a) to **(c)** shows the steady-state three-phase stator line voltages and currents for the PMBLDC motor drive implemented on dSPACE MicroLab Box 1202. In this case, the P controller is employed as a speed controller. The voltage waveforms are in the form of pulses, whereas the current waveforms are near quasi-square waves. **Figure 14(d)** to **(f)** shows the three-phase stator line voltage and currents for the PMBLDC motor drive with the increase in load. The dynamic performance analysis reveals that with the increase in load, the current also increases to meet the load demand. However, the current does not exceed the maximum permissible value. Also, no abnormality is observed in the voltage waveform. **Figure 14(g)** shows the speed and load torque. The rotor speed tracks the reference speed. The reference speed is increased from 800 r/min to 1350 r/min and then to 1500 r/min. There are no overshoots, undershoots, or oscillations observed in the rotor speed. However, a steady-state error is observed. With the change in reference speed, the control system ensures that there is an increase in current to meet the increased load demand. Hence, the developed torque increases. As acceleration imposes increased load torque demand, there is a spike observed in the developed torque to ensure that the rotor speed accelerates. **Figure 14(h)** to **(i)** shows the output of the hall position sensors for phases a and b.

The steady-state three-phase stator line voltages and currents for the PMBLDC motor drive with PI speed controller developed on the dSPACE MicroLab Box 1202 platform are shown in **Figure 15(a)** to **(c)**. With a PI controller, the steady state speed error can be eliminated. While the current waveforms resemble quasi-square waves with some distortions, the voltage waveforms take the shape of pulses as per the PWM gate pulses applied to the inverter. The three-phase stator line voltage and currents for the PMBLDC motor drive observed under the increase in load are shown in **Figure 15(d)** to **(f)**. According to the dynamic performance analysis, as the load is increased, the magnitude of the current must also increase to keep up with the demand. The current does not, however, go above the maximum value allowed. Additionally, there are no anomalies in the voltage waveform. The load torque and speed are displayed in **Figure 15(g)**. The rotor speed follows the reference speed exactly. After increasing from 800 r/min to 1350 r/min, the reference speed is then raised to 1500 r/min. There is a small overshoot in rotor speed as it is increased from 800 r/min to 1350 r/min. It is to be noted that the rotor speed does not exhibit any oscillations. No overshoot is observed when the speed is increased from 1350 r/min to 1500 r/min. The control system makes sure that, with the change in reference speed, there is an increase in current to handle the increased load demand. Consequently, the developed torque rises. There is a spike in the produced torque that is detected to ensure that the rotor speed accelerates when acceleration imposes an increased load torque demand. The output of the hall position sensors for phases a and b is shown in **Figure 15(h)** to **(i)**.

With the PI speed controller, though the steady state error was eliminated, overshoot was observed in rotor speed. Also, distortions are observed in the start currents. To further improve the drive performance, PMBLDC drive operation is analyzed with a PID speed controller. **Figure 16(a)** to **(c)** displays the steady-state three-phase stator line voltages and currents obtained when the PID speed controller is used in the PMBLDC motor drive built on the dSPACE MicroLab Box 1202 platform. The voltage waveforms take the form of pulses following the PWM gate pulses applied to the inverter, whilst the current waveforms resemble

quasi-square waves. The distortions observed in stator currents with the PI speed controller are eliminated. **Figure 16(d)** to **(f)** illustrates the three-phase stator line voltage and currents for the PMBLDC motor drive measured under the increased load. The dynamic performance study indicates that as the load is raised, the current magnitude must also grow to meet the demand. The current stays below the permitted maximum value, nevertheless. The voltage waveform is also free of any abnormalities. **Figure 16(g)** displays the load torque and actual rotor speed. Reference speed is exactly tracked by the rotor speed. The reference speed is increased from 800 r/min to 1350 r/min and subsequently increased to 1500 r/min. As the rotor speed rises from 800 to 1350 r/min, no overshoot, which was observed in the earlier case, is observed. The derivative action ensures the elimination of the overshoot. It should be noted that no other abnormalities are observed in the rotor speed. This remains true, even when the speed is raised from 1350 r/min to 1500 r/min. The control system makes sure that when the reference speed changes, an increase in current is made to suit the increasing load requirement. The increased stator current is to facilitate the increase in torque production to meet the load demand. As the load torque increases significantly while accelerating, Thus, the control system makes sure that an increase in current is made in response to the change in reference speed to accommodate the increased load demand. Therefore, to ensure that the rotor speed increases when acceleration imposes a higher load torque demand, a spike in the produced torque is monitored. **Figure 16(h)** to **(i)** displays the output of the hall position sensors for phases a and b. The hardware results presented in this work are in line with the simulation studies presented.

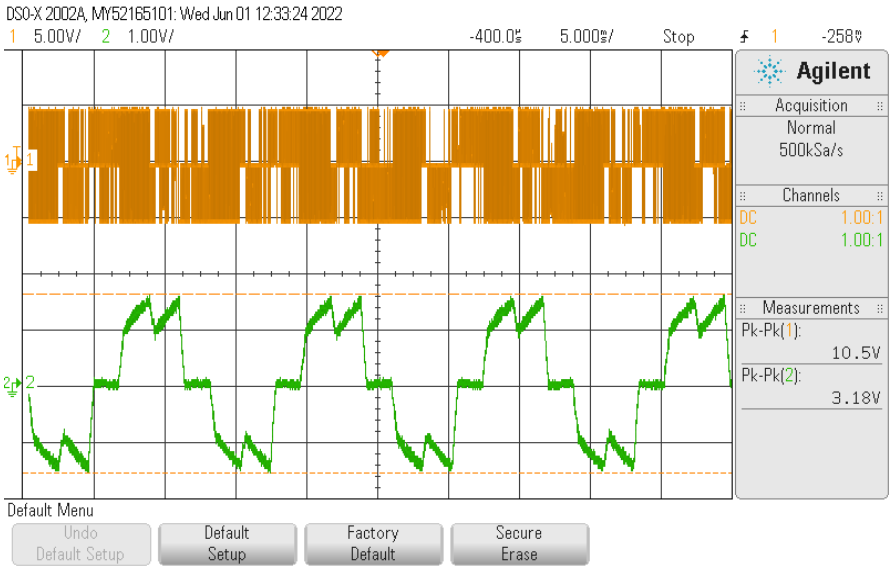

(a)

Figure 14. (*Continued*).

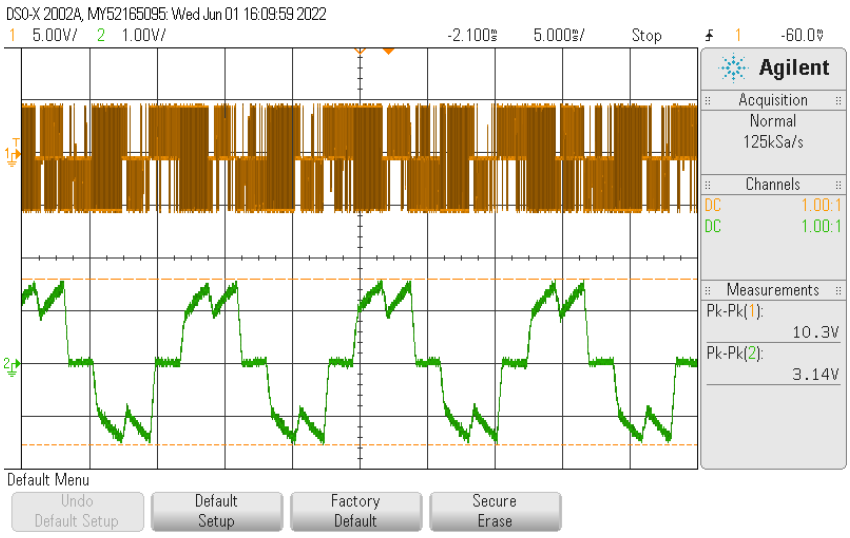

(b)

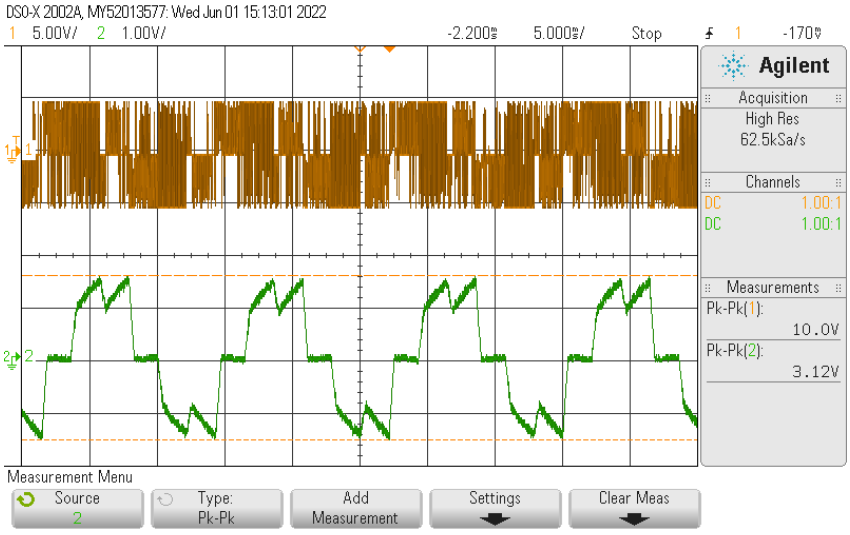

(c)

(d)

Figure 14. (*Continued*).

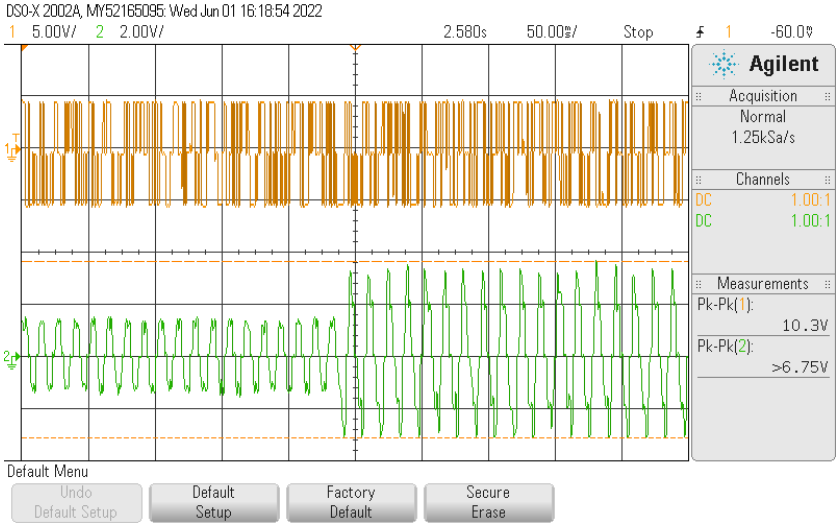

(e)

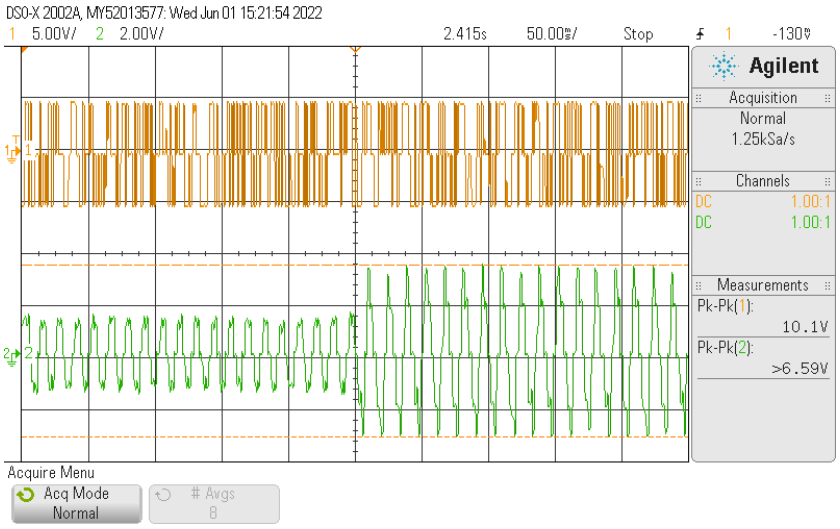

(f)

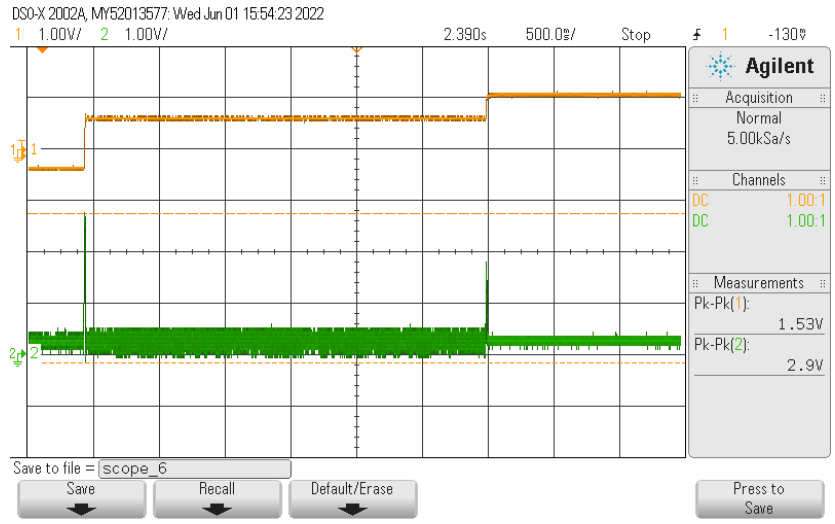

(g)

Figure 14. (*Continued*).

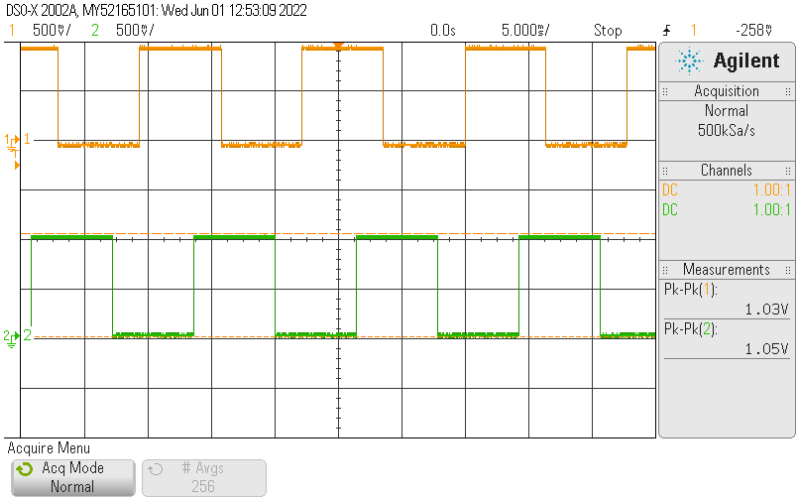

(h)

Figure 14. dSPACE results for solar PV array powered speed control of PMBLDC motor drive using "P" controller: **(a)** Vab & Ia, **(b)** Vbc & Ib, **(c)** Vca & Ic—under constant loading conditions, **(d)** Vab & Ia, **(e)** Vbc & Ib, **(f)** Vca & Ic—under variable loading conditions, **(g)** speed & torque, and **(h)** Ha & Hb.

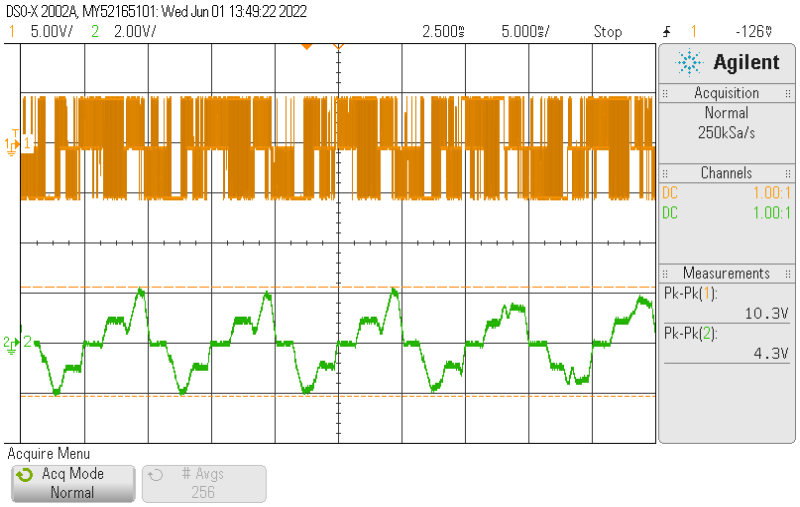

(a)

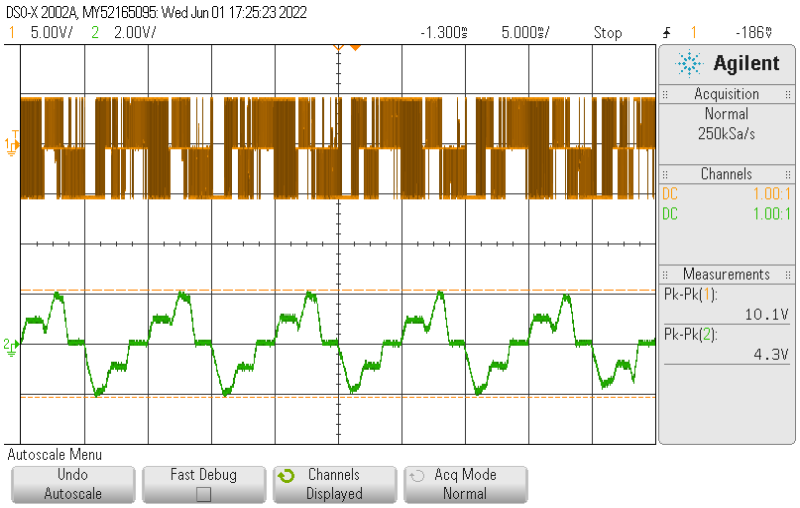

(b)

Figure 15. (*Continued*).

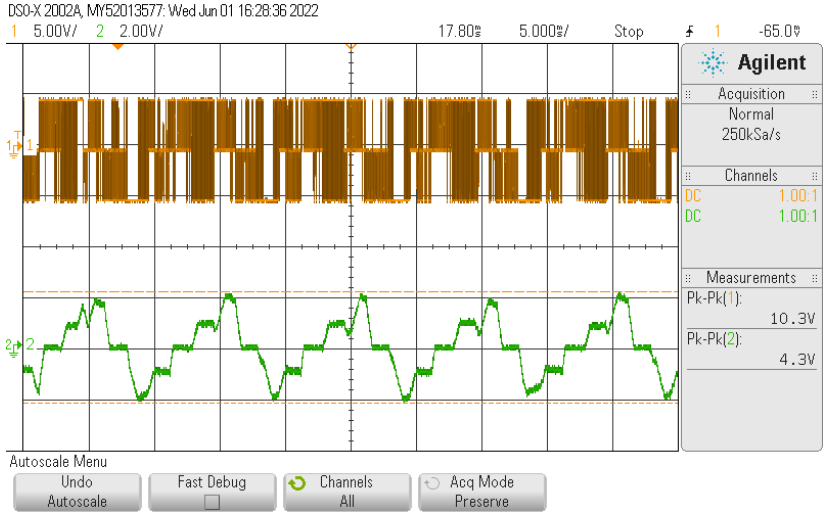

(c)

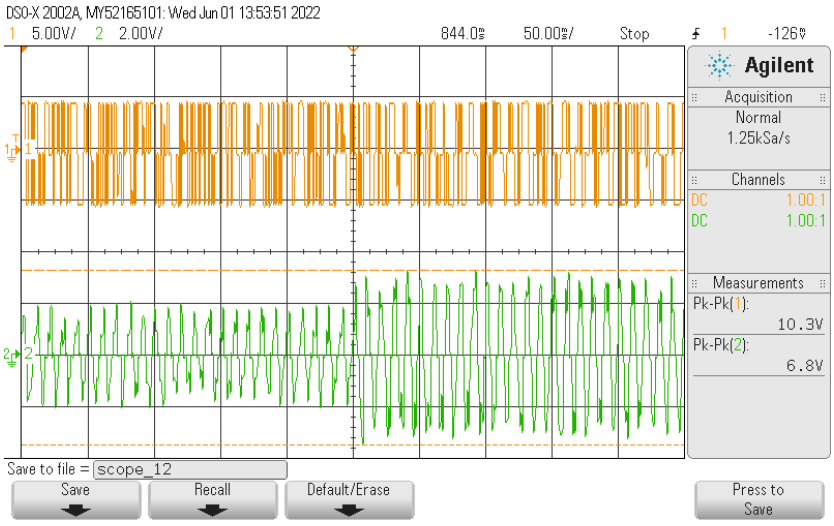

(d)

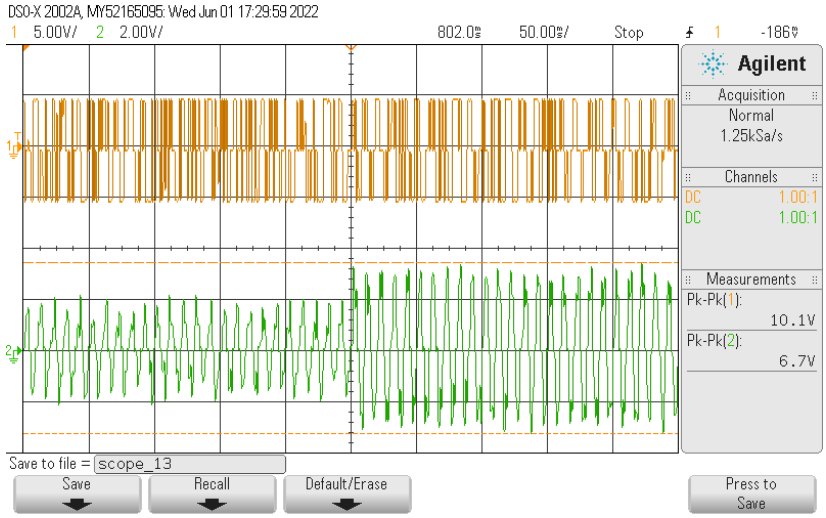

(e)

Figure 15. (*Continued*).

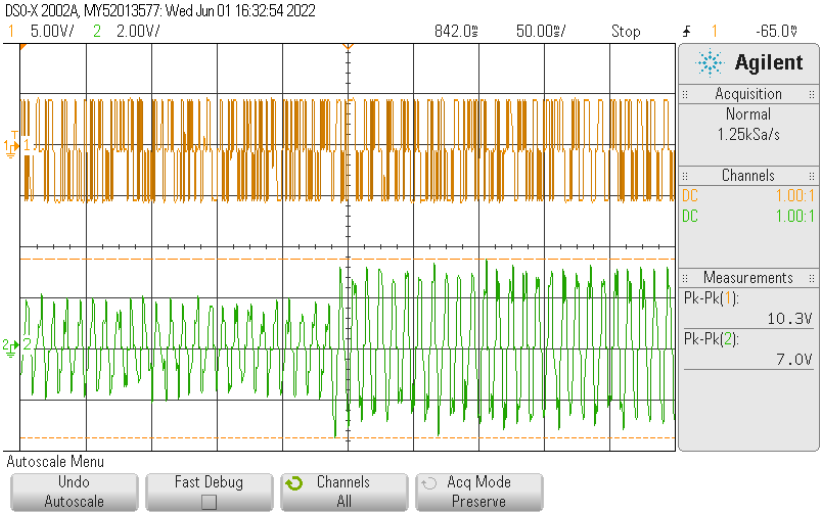

(f)

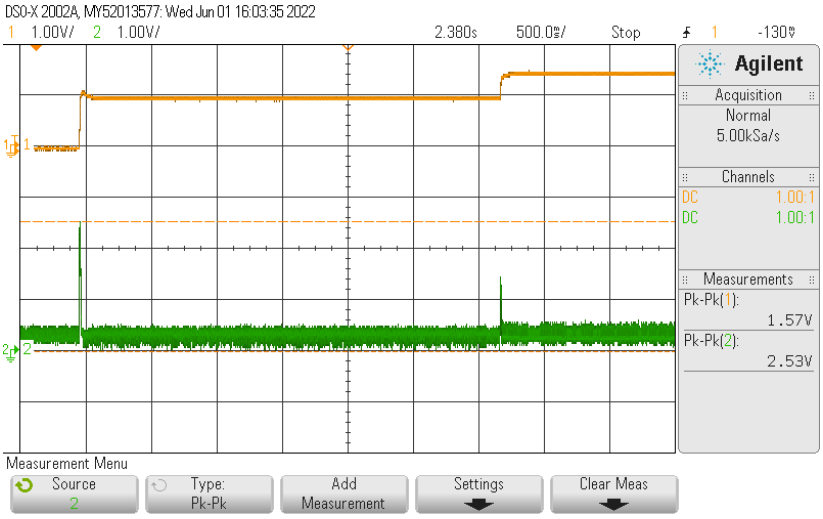

(g)

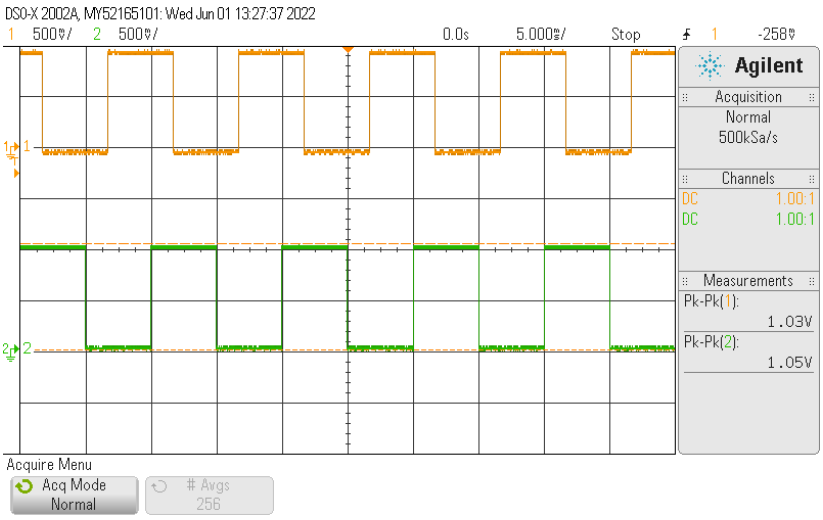

(h)

Figure 15. dSPACE results for solar PV array powered speed control of PMBLDC motor drive using "PI" controller: **(a)** Vab & Ia, **(b)** Vbc & Ib, **(c)** Vca & Ic—under constant loading conditions, **(d)** Vab & Ia, **(e)** Vbc & Ib, **(f)** Vca & Ic—under variable loading conditions, **(g)** speed & torque, and **(h)** Ha & Hb.

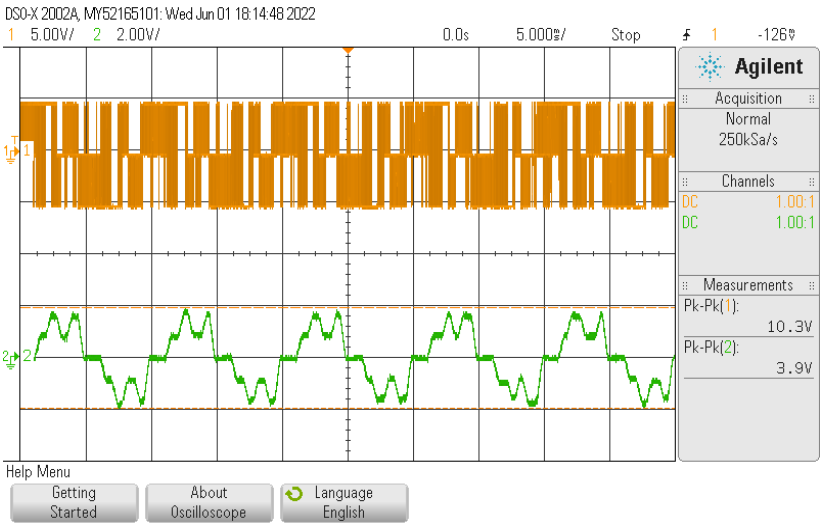

(a)

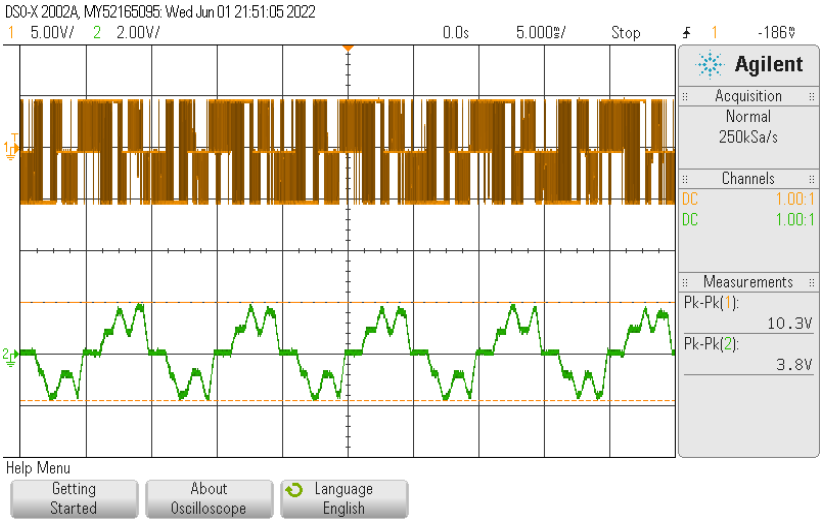

(b)

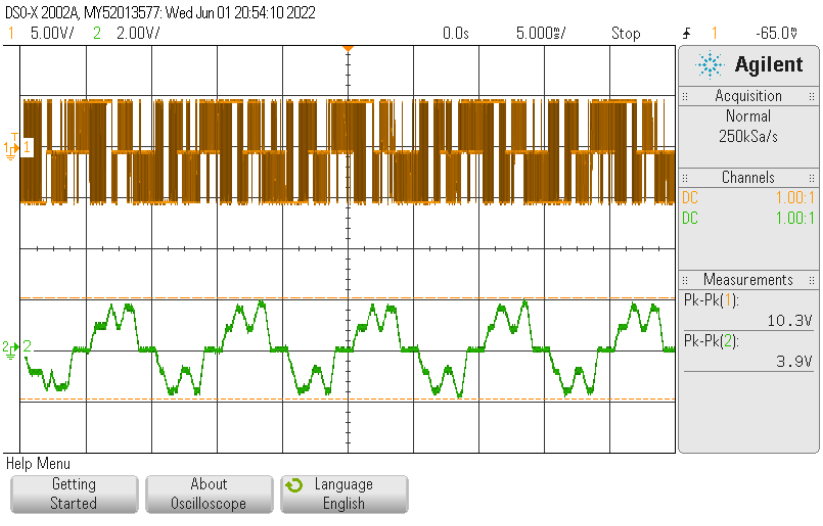

(c)

Figure 16. (*Continued*).

(d)

(e)

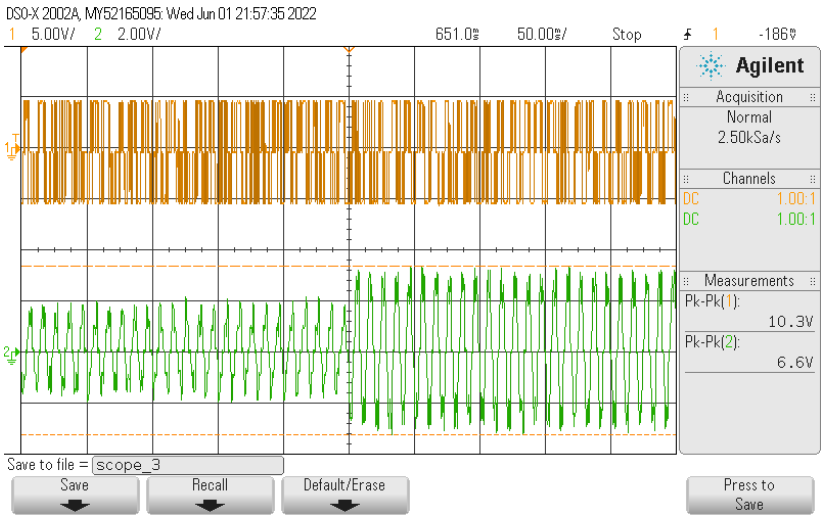

(f)

Figure 16. (*Continued*).

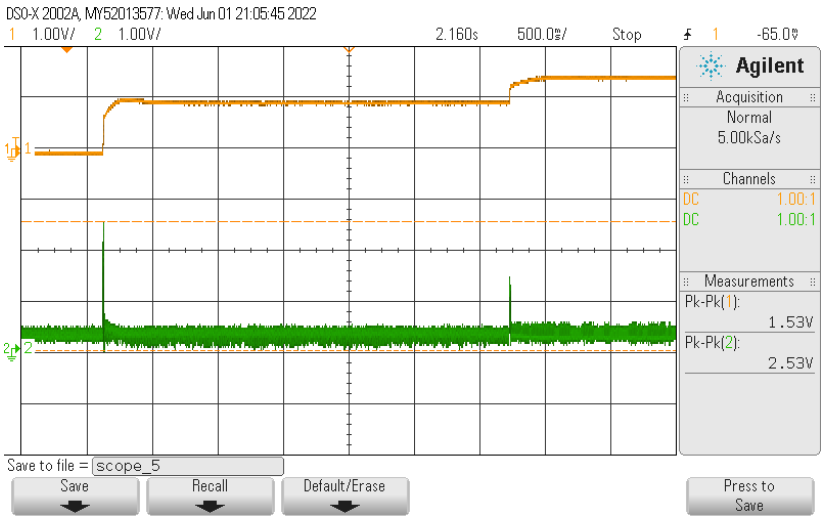

(g)

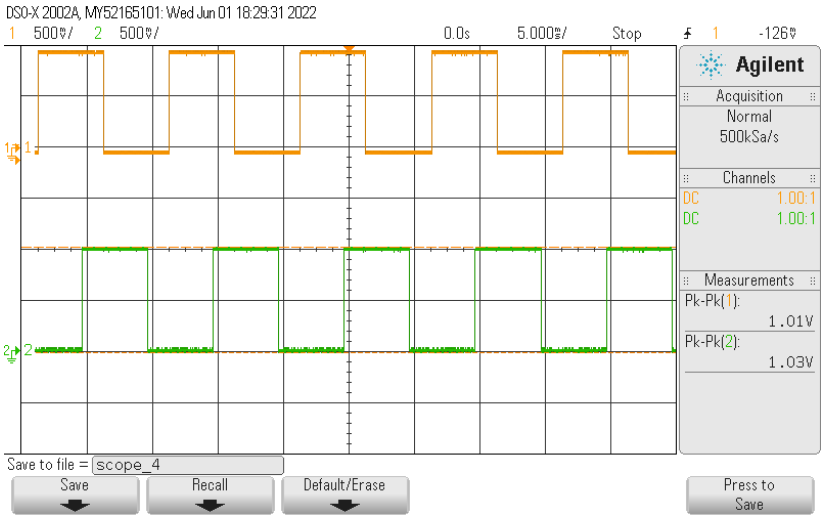

(h)

Figure 16. dSPACE results for solar PV array powered speed control of PMBLDC motor drive using "PID" controller: **(a)** Vab & Ia, **(b)** Vbc & Ib, **(c)** Vca & Ic—under constant loading conditions, **(d)** Vab & Ia, **(e)** Vbc & Ib, **(f)** Vca & Ic—under variable loading conditions, **(g)** speed & torque, and **(h)** Ha & Hb.

8. Conclusion

The performance of a solar PV array-powered PMBLDC motor drive is analyzed through simulation studies and hardware-in-loop implementation. P, PI, and PID controllers are employed as speed controllers. The system performance with these controllers is analyzed under constant load and variable load conditions. With the P controller, steady state speed error is observed. This issue can be resolved with the PI controller through integral action. However, with the PI controller current, distortions in stator currents and overshoot in the actual speed are observed. With the inclusion of derivative action, the problem of distortions in stator currents and overshoot in rotor speed can be eliminated. With this PID controller, torque ripples have been reduced considerably, and also overshoot, undershoot in speed has been reduced. Hence, PID controller is ideally suited for the solar PV array-powered PMBLDC motor drive.

Author contributions

Conceptualization, SKD and SBRC; methodology, SKD and SBRC; software, SKD; validation, AM, SKD, SBRC, and AVS; formal analysis, SKD and SBRC; investigation, SKD and SBRC; resources, SKD and SBRC; data curation, SKD, SBRC, and AVS; writing—original draft preparation, SKD and SBRC; writing—review and editing, SKD and AM; visualization, SKD and SBRC; supervision, AVS and AM; project administration, AVS. All authors have read and agreed to the published version of the manuscript.

Conflict of interest

The authors declare no conflict of interest.

References

1. Mani P, Mahadevan SK, Johnson AR, Kullan M. An optimized design modeling of PV integrated SEPIC-based four-switch inverter for sensorless PMBLDC motor control. *Automatika* 2022; 63(1): 90–101. doi: 10.1080/00051144.2021.2008621
2. Sen A, Singh B. Peak current detection starting based position sensorless control of BLDC motor drive for PV array fed irrigation pump. *IEEE Transactions on Industry Applications* 2021; 57(3): 2569–2577. doi: 10.1109/TIA.2021.3066831
3. Murshid S, Singh B. Implementation of PMSM drive for a solar water pumping system. *IEEE Transactions on Industry Applications* 2019; 55(5): 4956–4964. doi: 10.1109/TIA.2019.2924401
4. Rathore KS, Kalla UK, Bhati N, Palwalia DK. Solar PV array fed modified PMBLDCM drive scheme for blower applications. In: Proceedings of 2021 International Conference on Sustainable Energy and Future Electric Transportation (SEFET); 21–23 January 2021; Hyderabad. pp. 1–6.
5. Huang J, Fang H, Wang J. A PI controller optimized with modified differential evolution algorithm for speed control of BLDC motor. *Automatika* 2019; 60(2): 135–148. doi: 10.1080/00051144.2019.1596014
6. Swamy CLP, Singh B, Singh BP, Murthy SS. Experimental investigations on a permanent magnet brushless DC motor fed by PV array for water pumping system. In: Proceedings of the 31st Intersociety Energy Conversion Engineering Conference; 11–16 August 1996; Washington. pp. 1663–1668.
7. Panda A, Kahare S, Gawre SK. DSP TMS320F28377S based speed control of DC motor. In: Proceedings of 2020 IEEE International Students' Conference on Electrical, Electronics and Computer Science (SCEECS); 22–23 February 2020; Bhopal. pp. 1–4.
8. Kumar DD, Babu C, Reddy KJ, et al. An improved P&O MPPT control algorithm for increasing power extraction efficiency of solar PV module. *IOP Conference Series: Materials Science and Engineering* 2019; 623(1): 012020. doi: 10.1088/1757-899X/623/1/012020
9. Malla SG. Small signal model of PV power generation system. In: Proceedings of 2017 IEEE International Conference on Power, Control, Signals and Instrumentation Engineering (ICPCSI); 21–22 September 2017; Chennai. pp. 3069–3073.
10. Ghosh A, Malla SG, Bhende CN. Small-signal modeling and control of photovoltaic-based water pumping system. *ISA Transactions* 2015; 57: 382–389. doi: 10.1016/j.isatra.2015.01.008
11. Hussain AM, Habbi HM. Maximum power point tracking photovoltaic fed pumping system based on PI controller. In: Proceedings of 2018 Third Scientific Conference of Electrical Engineering (SCEE); 19–20 December 2018; Baghdad. pp. 78–83.
12. Hake P, Ugale RT. Solar PV and grid interfaced BLDC motor drive system for agricultural pump application. In: Proceedings of 2021 National Power Electronics Conference (NPEC); 15–17 December 2021; Bhubaneswar. pp. 1–6.
13. Kumar R, Singh B. BLDC motor driven water pump fed by solar photovoltaic array using boost converter. In: Proceedings of 2015 Annual IEEE India Conference (INDICON); 17–20 December 2015; New Delhi. pp. 1–6.
14. Gadekar K, Joshi S, Mehta H. Performance improvement in BLDC motor drive using self-tuning PID controller. In: Proceedings of 2020 Second International Conference on Inventive Research in Computing Applications (ICIRCA); 15–17 July 2020; Coimbatore. pp. 1162–1166.
15. Shanmugasundram R, Zakariah KM, Yadaiah N. Implementation and performance analysis of digital controllers for brushless DC motor drives. *IEEE/ASME Transactions on Mechatronics* 2012; 19(1): 213–224. doi: 10.1109/TMECH.2012.2226469

16. Niapour SK, Danyali S, Sharifian MB, Feyzi MR. Brushless DC motor drives supplied by PV power system based on Z-source inverter and FL-IC MPPT controller. *Energy Conversion and Management* 2011; 52(8–9): 3043–3059. doi: 10.1016/j.enconman.2011.04.016
17. Sharma PK, Sindekar AS. Performance analysis and comparison of BLDC motor drive using PI and FOC. In: Proceedings of 2016 International Conference on Global Trends in Signal Processing, Information Computing and Communication (ICGTSPICC); 22–24 December 2016; Jalgaon. pp. 485–492.
18. Saha B, Singh B. An economical approach for solar PV-battery based E-rickshaw with regenerative braking using sensorless BLDC motor drive. In: Proceedings of 2020 IEEE International Conference on Power Electronics, Drives and Energy Systems (PEDES); 16–19 December 2020; Jaipur. pp. 1–6.
19. Shyam A, Daya JLF. A comparative study on the speed response of BLDC motor using conventional PI controller, anti-windup PI controller and fuzzy controller. In: Proceedings of 2013 International Conference on Control Communication and Computing (ICCC); 13–15 December 2013; Thiruvananthapuram. pp. 68–73.
20. Madichetty S, Pullaguram D, Mishra S. A standalone BLDC based solar air cooler with MPP tracking for improved efficiency. *CSEE Journal of Power and Energy Systems* 2019; 5(1): 111–119. doi: 10.17775/CSEEJPES.2018.00410